Amorphous WO_3 as transparent conductive oxide in the Near-IR

Hao Chen[a,b]*, *Alice Carlotto*[c,d], *Cristina Armellini*[c], *Marco Cassinelli*[b], *Mario Caironi*[b], *Mohamed Zaghloul*[a,b], *Alberto Tagliaferri*[a,b], *Alessandro Chiasera*[d], *Silvia M. Pietralunga*[b,d]

[a]*Politecnico di Milano, Department of Physics, Piazza Leonardo da Vinci, 32, 20133 Milano, Italy*

[b]*CNST@PoliMi, Istituto Italiano di Tecnologia (IIT), Via Giovanni Pascoli 70/3, Milano, Italy*

[c]*IFN-CNR CSMFO Laboratory and FBK Photonics Unit, Via alla Cascata 56/C Povo 38123 Trento, Italy*

[d]*Institute for Photonics and Nanotechnologies (IFN)—National Research Council (CNR), Piazza L. da Vinci, 32, 20133 Milano, Italy*

ABSTRACT

The demand for transparent conductive films (TCFs) is dramatically increasing. In this work tungsten oxide (WO_{3-x}) is studied as a possible option additional to the existed TCFs. We introduce WO_{3-x} thin films fabricated by a non-reactive magnetron RF-sputtering process at room temperature, followed by thermal annealing in dry air. Films are characterized morphologically, structurally, electrically, optically, and dielectrically. Amorphous WO_{3-x} thin films are shown to be n-type conductive while the transparency extends to the near-IR. By evaluating a figure of merit for transparent-conductive performance and comparing to some most-widely used TCFs, WO_{3-x} turns out to outperform in the near-IR optical range.

Keywords: RF-sputtering, amorphous tungsten oxide, transparent conductive films, near-infrared

1. INTRODUCTION

Transparent conductors, which simultaneously require the high transmission of optical light and electric current, have been widely used in a variety of advanced applications, including information displays[1], light-emitting diodes[2], photovoltaic modules[3], and smart windows[4]. In recent years with the fast-growing market demand, the consumption of transparent and conductive films (TCFs) is dramatically increased. This trend is believed to become even more intense in the coming years. In this situation, various classes of transparent and conductive materials have been investigated, and some of them have reached good commercial availabilities. Among the different available categories of transparent conductors, metal oxides have gained widespread attention and domination in the markets. Indium tin oxide (ITO), due to its very low electrical resistivity (of the order of 10^{-4} $\Omega\cdot$cm) and very high optical transmittance (>85%) from visible to near-ultraviolet spectral range, is probably the best transparent conductive oxide (TCO) in market today[5]. However, this kind of notably well-performed TCO is also facing some intractable problems, apart from its high prices: difficulties in fabrication due to its instability with temperature and the presence of hydrogen[6]; relative high risk of long-term sustainability, due to rarity of indium element and its low recycling rate; as well as the limited transparency in the near-infrared range. The competitive metal-oxide products such as impurity-doped zinc oxide[7] and tin oxide[8], and other categories including conductive polymers and nanostructures[9], although have reached various degrees of success, are confronted with different unsatisfactory questions like durability, flexibility and so on.

In this study, tungsten oxide (WO_3) thin films are analyzed as a new type of TCO additional to the existed TCFs, and for compensating the shortcomings of ITO. WO_3 is a multi-functional semiconducting material that exhibits wide polymorphism and stoichiometries[10]. By manipulating the tungsten-to-oxygen compositional ratio and the microstructure, the material can be modulated to show a variety of interesting properties, thus applying to many different applications such as smart windows[4], gas sensors[11], as well as photo-electro and chemical uses[12]. Co-existence of good optical transparency in the near-infrared and electric conduction can also be obtained from oxygen deficient tungsten oxide (WO_{3-x})[13]. For WO_{3-}

*hao.chen@polimi.it; phone +39 3383677077

x thin films preparation, magnetron radio-frequency (RF) sputtering is adopted among the various possible film-growth methods for its high stability and controllability. Post-thermal annealing treatments in dry air are followed after deposition to modify the structure and stoichiometry of the material, therefore optimizing the balance between light transmission and current transport. Characterizations in morphological, structural, electrical, optical, and dielectric aspects are carried out to rate the transparent and conductive performance of WO_{3-x} thin films in comparison with some popular and commercially available TCOs.

2. EXPERIMENTAL SECTION

2.1 Sample preparation

WO_{3-x} thin films were deposited on fused silica slide and doped silicon wafer substrates through non-reactive magnetron RF-sputtering in argon atmosphere[14]. Before starting the deposition, ethanol rinse and pre-chamber heating at 120 °C for 10 min in vacuum were conducted to clean the substrates. Then the two substrates were simultaneously transferred into the deposition chamber, bearing the same film-growth environment, therefore forming nominally the identical WO_{3-x} thin films. A stoichiometric WO_3 target with purity higher than 99.9% was place at a distance of 25 cm away from the substrates. The target was pre-sputtered for about 10 mins to ensure no contaminants would be mixed to the film. Growth of the WO_{3-x} films started when the chamber pressure was stabilized at $5.4 \cdot 10^{-3}$ mbar and power at 81 W. During the sputtering, both target and substrates were kept at room temperature with the cooling system. Figure 1 simply shows the scheme of RF-sputtering for depositing WO_{3-x} thin films.

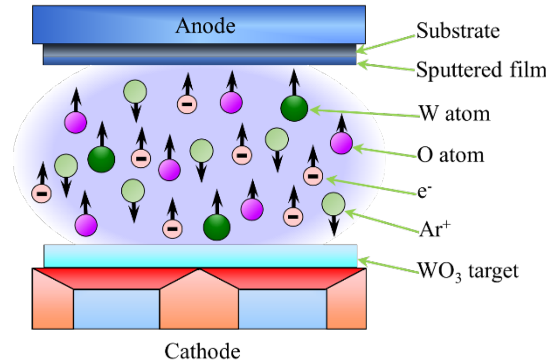

Figure 1. Schematic representation of RF-sputtering for depositing WO_{3-x} thin films.

After deposition, samples were divided equally into three pieces and brought two of them to the thermal annealing treatments. Annealing temperature at 300 °C was selected, which is below the crystallization temperature for WO_3[15]. For comparison, annealing at a temperature above the crystallizing transition was also performed (400 °C). All the post-thermal treatments were carried out in dry air for 8 hours. Eventually three samples were prepared for the study, namely the as-deposited, the annealed at 300 °C and the annealed at 400 °C, and each sample was prepared on two different substrates.

2.2 Characterization methods

The assessment of the prepared WO_{3-x} thin films was performed from morphological, structural, electrical, optical, and dielectric aspects. High-resolution scanning electron microscope (SEM, Tescan MIRA3) and atomic force microscope (AFM) in taping mode were applied to samples deposited on Si substrate, in order to evaluate the thickness, morphology, and surface roughness of the films. Structures regarding the degree of atomic periodicity was determined by means of X-ray diffraction (XRD, Panalytical X'Pert Pro) using samples deposited on Si substrate. Sheet resistance was tested with samples deposited on fused silica substrate in direct current (DC) mode at room temperature, using 4-probe method in Van der Pauw configuration[16]. Optical transmittance from ultraviolet (UV) to near-infrared (NIR) was characterized with samples deposited on glass substrate by UV-NIR spectrophotometer (Varian-Cary 5000). Optical constants in the spectral range from 350 nm to 1700 nm of the films were retrieved through variable angle spectroscopic ellipsometry (VASE, J.A. Woollam Co.,Inc.), using samples on both substrates. Models were built accordingly to fit the VASE data and thus extracting the dielectric functions.

3. RESULTS AND DISCUSSION

3.1 Morphology and structure

The SEM cross-sectional image for the as-deposited WO_{3-x} thin film is shown in Figure 2(a), indicating its smoothness, compactness, and good attachment to the substrate. Thickness is estimated to be around 90 nm and is not varied by the post-thermal treatments. Figure 2(b) shows the SEM image for the sample annealed at 300 °C at the front view. The artificial defect verifies the plane of focus on the sample surface, but no feature is observed. The as-deposited sample shows the same featureless surface, thus it is not presented here. Conversely, the annealed sample at 400 °C in Figure 2(c) presents clear grains, in good agreement with the AFM image and XRD pattern shown below.

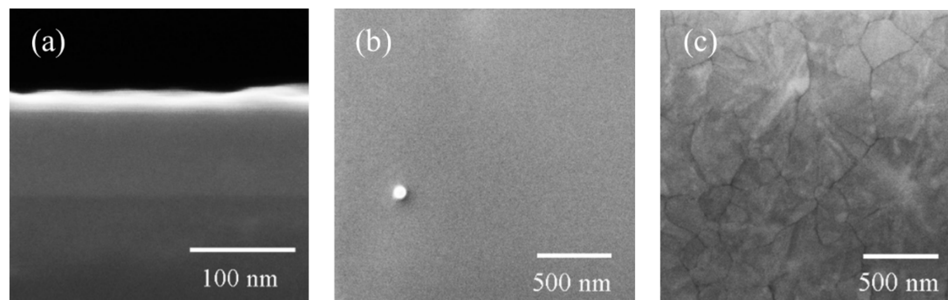

Figure 2. SEM images for the WO_{3-x} thin films:(a) SEM cross-sectional image for the as-deposited sample; (b) SEM surficial image for the annealed sample at 300 °C; (c) SEM surficial image for the annealed sample at 400 °C.

Surface morphology and roughness of the WO_{3-x} thin films were analyzed through AFM. Scans were taken over 4 μm^2 area at different spots. Figure 3 illustrates the AFM topography images for the as-deposited and posted-annealed WO_{3-x} thin films. Figure 3(a) and 3(b), correspond to the as-deposited and annealed sample at 300 °C, respectively. AFM images for both these samples highlight a very uniform surface and an extremely low roughness (root mean squared roughness R_q < 1 nm). Figure 3(c) shows some specific features that can also be found from the SEM image of the same sample annealed at 400 °C. The discussion on this part is not going to expand in this work. However, surface roughness results to be a bit higher by annealing at 400 °C (R_q < 2 nm), comparing to the previous two cases.

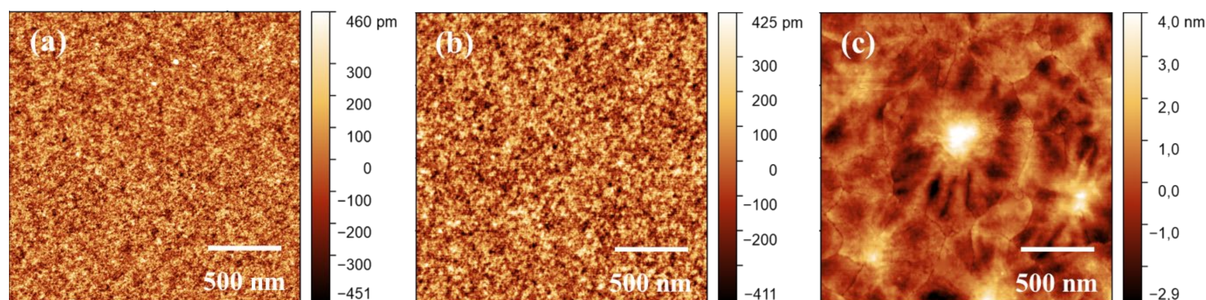

Figure 3. AFM topography images for the as-deposited (a), annealed at 300 °C (b), and annealed at 400 °C (c) WO_{3-x} thin films. The color bar indicates the vertical distance between peaks and valleys of roughness.

Figure 4 reports the XRD patterns of as-deposited and post-annealed samples over the angle range 20°~100°. Small humps centered at around 24° and 68° in all three traces are believed to be caused by the Si substrate. For the as-deposited sample, the XRD pattern looks rather smooth, suggesting its amorphous structure, that is, the absence of long-range order of atomic periodicity. Annealing at 300 °C does not promote the formation of evident peaks, thus as expected, amorphous state is remained in this case. In contrast, narrow and sharp peaks appears when the heat-treatment temperature rises to 400 °C. These peaks dominantly centered at 23.175° and 34.025° match the monoclinic phase, space group P21/n, according to JCPDS 72-1465. Results are consistent with the elsewhere reports[14].

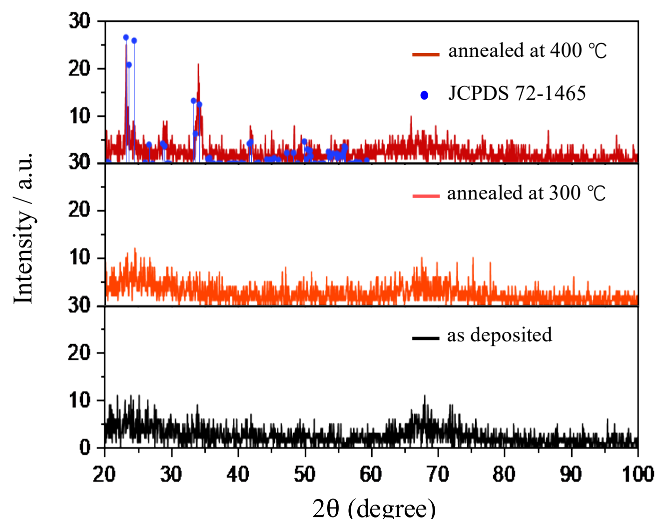

Figure 4. XRD patterns for the RF-sputtered WO_{3-x} thin films with and without post-thermal treatments.

3.2 Optical and dielectric responses

The as-deposited sample exhibits a dark blue, which is the typical color of sub-stoichiometric WO_{3-x}. Transparency is increased by annealing, as the dark color fades with annealing temperature, and eventually turns to yellowish when annealing temperature is raised to 400 °C. Figure 5 shows the spectral transmittance of the WO_{3-x} thin films in the range from UV to NIR. Transmittance is almost doubled with thermal treatments comparing to the as-deposited sample. Both annealed samples reach around 80% of transmittance in the NIR, while the as-deposited sample transmits only about 40% of NIR light. A higher annealing temperature results in a better optical transmission, but the contribution is very limited.

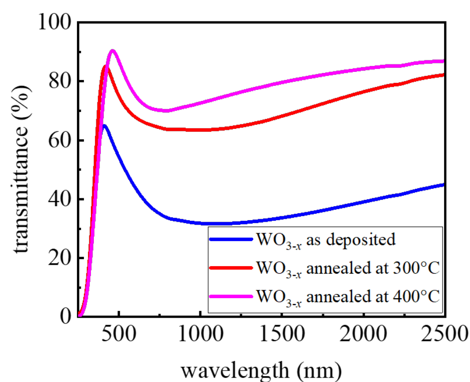

Figure 5. Spectral transmittance for the RF-sputtered WO_{3-x} thin films at different post-growth processing conditions.

The differently treated WO_{3-x} thin films are furtherly analyzed for their dielectric dispersions using VASE ellipsometry. Firstly, the two substrates are characterized in the same spectroscopic range as the WO_{3-x} samples and simple models are built. For silicon wafer substrate, the pseudo refractive index (n) and extinction coefficient (k) are directly inverted from the experimental data and are used as a reference to model the general oscillator with Tauc-Lorentz and Gaussian functions. The strategy for fused silica substrate is different: transmittance is appended to the VASE fitting and a simple Cauchy function is used, where zero absorption in the examined spectral range is assumed. For WO_{3-x} samples, since films deposited on to different substrates are nominally identical, dielectric dispersion is assumed to be the same. In this case in order to optimize the modeling, the results of fitting from samples deposited on Si substrate (WO_{3-x}_Si) are saved as a reference for modeling the counterpart deposited on fused silica substrate (WO_{3-x}_SiO_2). The as-deposited WO_{3-x}_Si is modeled simply with Gaussian functions starting from the pseudo n and k. The obtained dispersion is then referred to the fitting of as-deposited WO_{3-x}_SiO_2 in appendence with optical transmission intensity, where Lorentz and Drude functions are employed. For the annealed WO_{3-x}_Si at 300 °C, zero absorption is assumed in the NIR, in which range a Cauchy

function is used to fix the film thickness. Subsequently n and k are directly fitted through point-by-point fitting and are used as a reference for a general oscillator that includes Tauc-Lorentz and Drude functions. The obtained dispersion relation is then applied to the fitting of annealed WO_{3-x}_SiO_2 at 300 °C, also appended with transmittance. In this final step Tauc-Lorentz and Drude functions are again used. In case of annealed sample at 400 °C, when fitting the film on Si substrate, an Urbach tail function is added in addition to Cauchy function in order to account for the absorption near the band gap. Then n and k are saved as a reference for modeling the annealed WO_{3-x}_SiO_2 at 400 °C, with only one Tauc-Lorentz function.

The final dielectric function dispersions for the three samples are shown in Figure 6, where the blue curve represents refractive index (n) and red curve represents extinction coefficient (k). Figure 6(a) and Figure 6(b), which correspond respectively to the as-deposited and the annealed sample at 300 °C, show the similar abnormal dispersions of refractive index and peaks of extinction coefficient in the NIR. The major difference between the two samples is that for the annealed film at 300 °C, the absorption peak is narrowed and reduced. Instead, the annealed sample at 400 °C shown in Figure 6(c) presents a normal dispersion relation, which is the typical dispersion shape for the dielectric materials, thus suggesting the dielectric nature of WO_{3-x} thin film annealed at 400 °C.

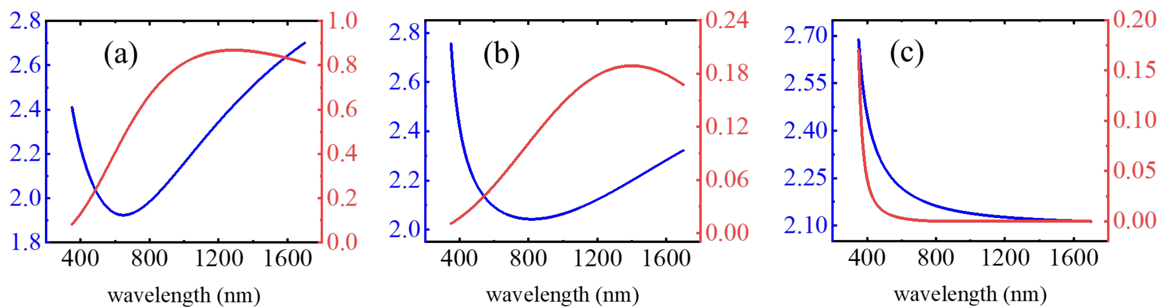

Figure 6. Dielectric functions for the as-deposited (a), annealed at 300 °C (b), and annealed at 400 °C (c) WO_{3-x} thin films. Blue curve represents refractive index (n) and red curve represents extinction coefficient (k).

3.3 Figure of merit

In order to quantitatively rate the transparent and conductive performance, various evaluation methods have been proposed[5,17,18]. Among the methods, the most popular evaluation way is based on Haacke's figure of merit (FOM)[18], the expression of which is shown in Equation 1,

$$\mathrm{FOM} = \frac{T^{10}}{R_s} \tag{1}$$

where T is the transmittance (%) and R_s is the sheet resistance (Ω/□). A larger value of FOM always suggests a better transparent-conductive performance. Sheet resistances for the three WO_{3-x} thin films are reported in Table 1.

Table 1. Sheet resistance and resistivity of the WO_{3-x} thin films at different post-processing conditions.

	sheet resistance	**resistivity**
as-deposited	7.4 kΩ/□	0.0666 Ω·cm
annealed at 300 °C	15 kΩ/□	0.135 Ω·cm
annealed at 400 °C	80 MΩ/□	720 Ω·cm

Figure 7 compares the logarithmic FOM of WO_{3-x} thin films in the NIR up to 2500 nm, with some popular and most-widely used TCFs, including ITO, aluminum-doped zinc oxide (AZO) and fluorine-doped tin oxide (FTO)[19,20]. The FOM for these popularly used TCFs starts to decay quickly when wavelength comes to NIR. Instead, the WO_{3-x} thin films show a steady enhancement of FOM as wavelength increases in the NIR, and eventually outperform tin oxide and zinc oxide at wavelength higher than 2000 nm. In particular, the amorphous WO_{3-x} thin films perform better than the crystallized one, and the annealed film at 300 °C shows the best transparent-conductive performance among the three samples.

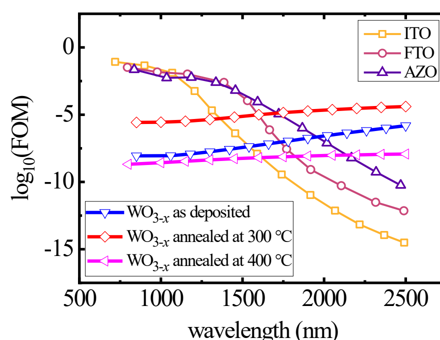

Figure 7. Logarithmic figure of merit for WO_{3-x} thin films based on Haacke's evaluation method, in comparison with ITO, FTO, and AZO[19,20].

4. CONCLUSIONS

Smooth and compact WO_{3-x} thin films with very low surface roughness are produced by a non-reactive magnetron RF-sputtering process. Post-thermal treatment in air at 400 °C promotes the crystallization of WO_{3-x} thin film, and make the film behave more dielectrically. At this annealing condition, both optical transparency and electrical resistivity increases dramatically, eventually the figure of merit that evaluates the transparent-conductive performance decreases. While post-annealing in air at 300 °C enhances the optical transparency and does not raise much the resistivity. Thus, amorphous WO_{3-x} thin film after low-temperature annealing behaves the best as a transparent and conductive film and is suitable for the near-infrared range.

ACKNOWLEDGEMENTS

Authors acknowledge co-funding of research by European fund - FESR, PON Ricerca e Innovazione 2014-2020, Project BEST4U – ARS01_00519.

REFERENCES

[1] Oh, B. Y. *et al.* "Transparent conductive Al-doped ZnO films for liquid crystal displays," *J. Appl. Phys.* **99**, 124505 (2006).
[2] Kim, H. *et al.* "Electrical, optical, and structural properties of indium-tin-oxide thin films for organic light-emitting devices," *J. Appl. Phys.* **86**, 6451–6461 (1999).
[3] Martínez, M. A., Herrero, J. & Gutiérrez, M. T. "Deposition of transparent and conductive Al-doped ZnO thin films for photovoltaic solar cells," *Sol. Energy Mater. Sol. Cells* **45**, 75–86 (1997).
[4] Niklasson, G. A. & Granqvist, C. G. "Electrochromics for smart windows: Thin films of tungsten oxide and nickel oxide, and devices based on these," *J. Mater. Chem.* **17**, 127–156 (2007).
[5] Ellmer, K., "Past achievements and future challenges in the development of optically transparent electrodes," *Nat. Photonics* **6**, 809–817 (2012).
[6] Major, S., Kumar, S., Bhatnagar, M. & Chopra, K. L. "Effect of hydrogen plasma treatment on transparent conducting oxides," *Appl. Phys. Lett.* **49**, 394–396 (1986).

[7] Minami, T. "Present status of transparent conducting oxide thin-film development for Indium-Tin-Oxide (ITO) substitutes," *Thin Solid Films* **516**, 5822–5828 (2008).

[8] Rakhshani, A. E., Makdisi, Y. & Ramazaniyan, H. A. "Electronic and optical properties of fluorine-doped tin oxide films," *J. Appl. Phys.* **83**, 1049–1057 (1998).

[9] Cao, W., Li, J., Chen, H. & Xue, J. "Transparent electrodes for organic optoelectronic devices: a review," *J. Photonics Energy* **4**, 040990 (2014).

[10] Mardare, C. C. & Hassel, A. W. "Review on the Versatility of Tungsten Oxide Coatings," *Phys. Status Solidi Appl. Mater. Sci.* **216**, 1900047 (2019).

[11] Di Giulio, M., Manno, D., Micocci, G., Serra, A. & Tepore, A. "Gas-sensing properties of sputtered thin films of tungsten oxide," *J. Phys. D. Appl. Phys.* **30**, 3211–3215 (1997).

[12] Zheng, G. *et al.* "Tungsten oxide nanostructures and nanocomposites for photoelectrochemical water splitting," *Nanoscale* **11**, 18968–18994 (2019).

[13] Chen, H. *et al.* "Near-IR transparent conductive amorphous tungsten oxide thin layers by non-reactive radio-frequency magnetron sputtering," EPJ Web of Conferences **255**, 05003 (2021).

[14] Chen, H. *et al.* "Tungsten oxide films by radio-frequency magnetron sputtering for near-infrared photonics," *Opt. Mater. X*, **12,** 100093 (2021).

[15] Kim, C.-Y. & Park, S. "Electrochromic properties of WO_3 thin film with various heat-treatment temperature," *Asian J. Chem.* **25**, 5874–5878 (2013).

[16] Van der Pauw, L. J. "A method of measuring specific resistivity and Hall effect of discs of arbitrary shape," *Philips Res. Reports* **13**, 1–9 (1958).

[17] Jain, V. K. & Kulshreshtha, A. P. "Indium-Tin-Oxide transparent conducting coatings on silicon solar cells and their 'figure of merit'," *Sol. Energy Mater.* **4**, 151–158 (1981).

[18] Haacke, G. "New figure of merit for transparent conductors," *J. Appl. Phys.* **47**, 4086–4089 (1976).

[19] Langley, D. *et al.* "Flexible transparent conductive materials based on silver nanowire networks: A review," *Nanotechnology* **24**, (2013).

[20] Noor, N. & Parkin, I. P. "Enhanced transparent-conducting fluorine-doped tin oxide films formed by Aerosol-Assisted Chemical Vapour Deposition," *J. Mater. Chem. C* **1**, 984–996 (2013).